physics

MDPI

Article

Dynamics of Neutron Transfer in the Reaction ^{3}He + ^{9}Be

Aidos K. Azhibekov [1,2], Englik K. Almanbetova [1], Mikhail A. Naumenko [1], Kairat O. Mendibayev [1,3,*], Sergey M. Lukyanov [1], Talgat G. Issatayev [1,4], Bakhytzhan A. Urazbekov [4], Asset M. Kabyshev [4,*], Kuralay Dyussebayeva [5] and Timur K. Zholdybayev [3]

1 Flerov Laboratory of Nuclear Reactions, Joint Institute for Nuclear Research, Dubna 141980, Russia; lukyan@jinr.ru (S.M.L.)
2 Department of Physics and Mathematics, Korkyt Ata Kyzylorda University, Kyzylorda 120014, Kazakhstan
3 Institute of Nuclear Physics, Almaty 050032, Kazakhstan
4 International Department of Nuclear Physics, New Materials and Technologies, L.N. Gumilyov Eurasian National University, Astana 010008, Kazakhstan
5 Theoretical and Nuclear Physics Department, Al-Farabi Kazakh National University, Almaty 050038, Kazakhstan; kura15@mail.ru
* Correspondence: kayrat1988@bk.ru (K.O.M.); assetenu@gmail.com (A.M.K.)

Abstract: The paper presents the results of experiments on measuring cross-sections for the neutron transfer channels ^{9}Be(^{3}He, α)^{8}Be$_{gs,3.03}$ in the reaction of the ^{3}He (30 MeV) ions with the ^{9}Be target. To describe the angular distributions, we use the Distorted Wave Born Approximation (DWBA) applying the FRESCO code. The results of the theoretical analysis are in agreement with the experimental data. In addition, we perform calculations based on the solution of the time-dependent Schrödinger equation (TDSE) for the weakly bound neutron of the ^{9}Be nucleus. The TDSE approach allows us to determine the dynamics of the neutron transfer process and calculate the probabilities for the transfer and removal of the neutron of the ^{9}Be nucleus in the ^{3}He + ^{9}Be reaction.

Keywords: neutron transfer; DWBA; FRESCO code; TDSE approach

Citation: Azhibekov, A.K.; Almanbetova, E.K.; Naumenko, M.A.; Mendibayev, K.O.; Lukyanov, S.M.; Issatayev, T.G.; Urazbekov, B.A.; Kabyshev, A.M.; Dyussebayeva, K.; Zholdybayev, T.K. Dynamics of Neutron Transfer in the Reaction ^{3}He + ^{9}Be. *Physics* **2024**, *6*, 1281–1293. https://doi.org/10.3390/physics6040079

Received: 13 September 2024
Revised: 29 October 2024
Accepted: 1 November 2024
Published: 21 November 2024

1. Introduction

Among stable weakly bound nuclei, the ^{9}Be nucleus is one of highest interest. The ^{9}Be nucleus has a Borromean structure in the ground state [1–5] and is typically represented as a system of two α-clusters and a neutron (n) [6–8]. For instance, the (α + n + α) structure of the ^{9}Be nucleus was considered in Refs. [9,10] using Feynman path integrals. Experimental studies [7,11,12] on the cluster channels of the decay of the nucleus ^{9}Be are also in favor of the (α + n + α) structure. However, with some probability, the nucleus ^{9}Be can be in a state corresponding to a two-particle structure, as evidenced by the results of experimental investigations [13,14], where it was shown that the nucleus ^{9}Be can decay through the two-particle channels ^{9}Be $\rightarrow$ n + ^{8}Be or ^{9}Be $\rightarrow$ α + ^{5}He. As soon as the ^{9}Be nucleus is stable, this nucleus is much more convenient to be investigated as compared to other Borromean nuclei.

Structural features of light nuclei are manifested in nucleon transfer reactions [15–19], for example, in the angular distributions of reaction products. The structure of the light nuclei d, ^{3}He, and α is well understood, and thus, these nuclei are often employed to induce direct reactions, either as beams or as targets [15–19].

The process of the neutron transfer in a reaction with the ^{9}Be nucleus is of interest due to the belief that the low binding energies of the neutron (1.666 MeV) and α-particle (2.462 MeV) should influence the dynamics and mechanism of the transfer. The interaction of deuterons and alpha particles with ^{9}Be at an energy of 10–30 MeV/nucleon has been studied taking into account ^{9}Be cluster structure in Refs. [20,21]. The interaction potential for the colliding nuclei was constructed within the framework of the double-folding model using a three-body wave function. Calculations with the double folding potential carried out within the optical model

(OM) and the Distorted Wave Born Approximation (DWBA) provided reasonable agreement between the theoretical cross-sections and the experimental data.

In our earlier investigations [16–21], we performed experimental and theoretical studies of the angular distributions of the products of nucleon and cluster transfer in the reactions d + ^{9}Be [17,20,21], ^{3}He + ^{9}Be [16,18], and ^{6}Li + ^{9}Be [19]. The obtained data were analyzed using the OM, the coupled reaction channel (CRC) method, and the DWBA. The analysis of the experimental data showed the sensitivity of the cross-sections to the potential parameters in the exit channels. In the papers of other authors [22–24], experimental data on the neutron transfer in the ^{9}Be(^{3}He, α)^{8}Be reaction channel were also analyzed within the DWBA.

This paper presents a study of the neutron transfer process in the ^{9}Be(^{3}He, α)^{8}Be reaction channel. To describe the mechanism and dynamics of this process, the data are analyzed using the DWBA [25–27] and the time-dependent Schrödinger equation (TDSE) approach [28–31]. A direct comparison of the theoretical description of the neutron transfer process (in the case considered here, in the ^{3}He + ^{9}Be reaction) within the framework of the stationary (DWBA) and time-dependent approaches (TDSE) is the challenge that we intend to tackle in this study. Each approach has its own advantages and disadvantages, but if combined, these methods complement each other. For this purpose, in the TDSE calculations, we used the values of the potential parameters obtained in the DWBA calculations for the ^{3}He + ^{9}Be entrance channel and for the initial neutron wave functions. The TDSE approach allows for both qualitative (reaction dynamics) and quantitative analysis of the neutron transfer process (probabilities of neutron transfer and neutron removal, reaction channel cross-sections) [32–34].

The study of the dynamics and mechanisms of nuclear reactions with the ^{9}Be nucleus is also of importance for applied research. For example, ^{9}Be can be used as a structural material for thermonuclear reactors [35,36], and the mechanisms of the ^{3}He + ^{9}Be reaction must be taken into account when designing a reactor structure and modeling the processes of burning a dense hot plasma with the d + ^{3}He combination of nuclei in a metal ^{9}Be cylindrical liner [36]. Additionally, ^{9}Be can also be used as a target for neutron sources due to the quite large cross-section of the ^{9}Be(p,n) reaction [37,38].

2. Experiment

The experiment was performed on the U-120M cyclotron of the Nuclear Physics Institute, Řež, Czech Republic [39]. The ions of the ^{3}He beam (30 MeV) were incident on a self-supporting ^{9}Be foil target (2 mg/cm^{2}, 99%). Carbon and oxygen contaminations of the target were not observed in energy spectra. The average beam current was 10–20 nA [18,40].

To identify reaction products, energy loss, ΔE, and residual energy, E_{r}, were measured by four telescopes (the (ΔE–E)-method). Each telescope consisted of three silicon-lithium detectors with thicknesses of 10 μm (ΔE_1), 100 μm (ΔE_2), and 3 mm (E_{r}) and was protected by a 5 mm thick Cu–Pb collimator and a circular hole of 3 mm diameter [18,40]. The energy resolution of the detectors was about 150–200 keV (full width at half maximum, FWHM). The telescopes were located at a distance of about 25 cm from the target and could be rotated around it in the angular range of θ_{lab} = 7°–63° with a step of 1°–2°.

A typical example of a two-dimensional product identification matrix obtained at an emission angle of θ_{lab} = 16° is shown in Figure 1a. One can see that atomic mass number, A, and atomic number, Z, of detected particles were unambiguously identified. The corresponding excitation energy spectrum of the ^{8}Be nucleus, which is a complementary product to the detected ^{4}He nucleus, is shown in Figure 1b. The first peak corresponds to the 0^{+} ground state of ^{8}Be; the second peak is the 2^{+} excited state. Thus, these two peaks confirm the corresponding reaction channels with the neutron transfer from ^{9}Be to ^{3}He. Thus, the technique used allowed us to measure the energy of the products, identify reaction channels, and obtain their corresponding differential angular distributions of the products.

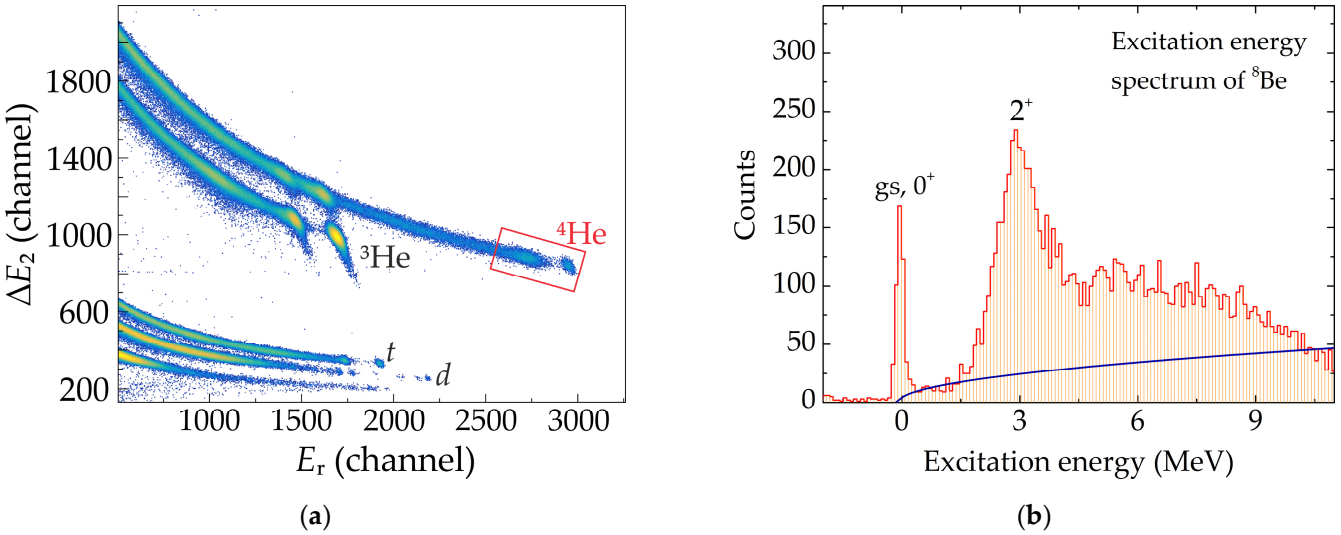

Figure 1. (**a**) A typical example of a two-dimensional product identification matrix obtained in the reaction ^{3}He + ^{9}Be at the laboratory energy E_{lab} = 30 MeV and the emission angle θ_{lab} = 16°. (**b**) The corresponding excitation energy spectrum of the ^{8}Be nucleus; the blue curve shows the background.

The outlined region in the (ΔE_2–E_r)-plot (Figure 1a) was used to obtain the excitation energy plot (Figure 1b). One can see that the 0^+ ground state of ^{8}Be and the 2^+ excited state are well separated. However, other reaction channels can contribute to the excitation energy plot in Figure 1b, in particular, the breakup of ^{8}Be, because it can undergo breakup with alpha particle emission. In the peak of the 0^+ ground state, the contribution of the background is insignificant. In the peak of the 2^+ excited state, the contribution of the background, mainly associated with the breakup process ^{8}Be → ^{4}He + ^{4}He with the threshold energy of –0.0918 MeV, is less than 15%; the contribution from the breakup of ^{9}Be is not present. To obtain the angular distributions presented in Section 3, the background contribution was subtracted.

Section 3 presents the theoretical analysis of the experimental data on the reaction channels ^{9}Be(^{3}He, α)^{8}Be$_{gs,3.03}$. Detailed information on other channels of the ^{3}He + ^{9}Be reaction can be found in our previous papers [18,40].

3. DWBA Calculations

Experimental differential cross-sections for neutron transfer in ^{9}Be(^{3}He, α)^{8}Be$_{gs,3.03}$ reaction channels are shown in Figure 2. To describe the experimental data, we used the prior formalism of the DWBA amplitude [25,26] and the FRESCO code [27]. To calculate the cross-sections of neutron (n) transfer reaction $A + b \rightarrow a + B$ ($A = a + n$, $B = b + n$), the formalism of the DWBA requires the potentials of the entrance and exit channels, the spectroscopic amplitudes S_x for the neutron in the systems $A = a + n$ and $B = b + n$, and the potentials for calculating the neutron wave functions within the shell model.

The values of the spectroscopic amplitudes S_x = 0.791 for ^{9}Be = ^{8}Be + n and S_x = –0.741 for ^{4}He = ^{3}He + n were taken from our previous study [18]. The neutron wave functions were calculated within the shell model using the potential in the Woods–Saxon form with geometric parameters $R = 1.25A^{1/3}$ fm (radius) and a = 0.65 fm (diffuseness); the potential depths were adjusted to reproduce binding energies of a neutron.

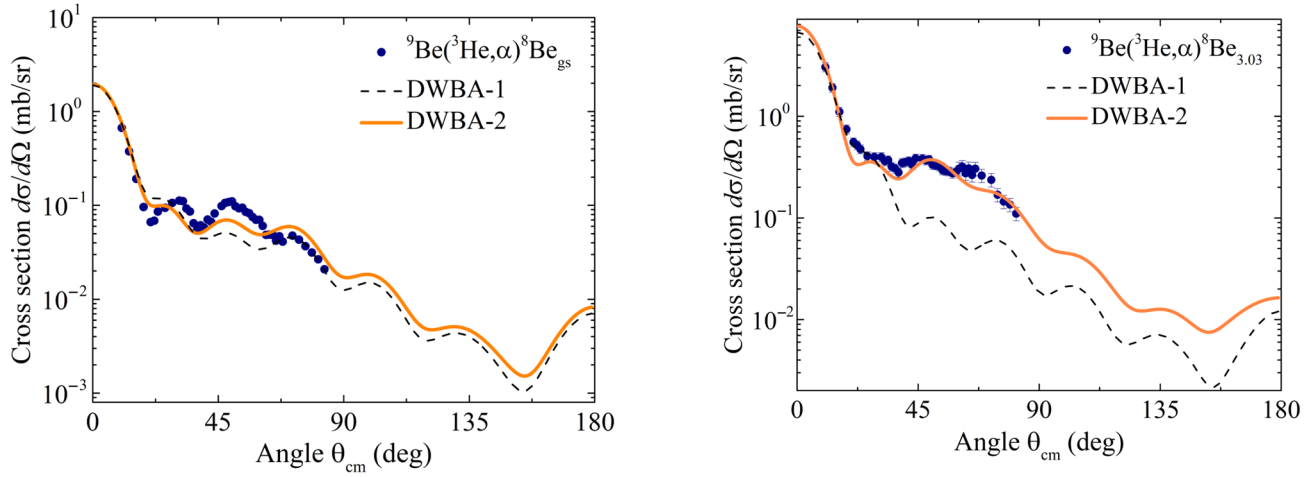

(**a**) (**b**)

Figure 2. Experimental angular distributions (circles) for the reaction channels (**a**) ^{9}Be(^{3}He, α)^{8}Be$_{gs}$ and (**b**) ^{9}Be(^{3}He, α)^{8}Be$_{3.03}$ compared with the results of calculations (curves) in the center of mass frame: DWBA-2 (with the potential parameters from Ref. [12]) and DWBA-1 (with the reduced depth of the imaginary part of the exit channel potential). See text for details.

As a starting point for searching for the optical potential U for the entrance and exit channels, we took the parameter sets from Ref. [18] (Table 1). These potential parameters have been successfully used to describe a number of experimental data on the nucleon and cluster transfer channels in the ^{3}He + ^{9}Be reaction. The potential U is defined as

$$U(r) = V_{C}(r) - V_{V} f(r; R_{V}, a_{V}) - iV_{W} f(r; R_{W}, a_{W}), \quad (1)$$

$$f(r; R_{V,W}, a_{V,W}) = \left[1 + \exp\left(\frac{r - R_{V,W}}{a_{V,W}}\right)\right]^{-1}, \quad (2)$$

$$R_{V,W} = r_{V,W}\left(A_{p}^{1/3} + A_{t}^{1/3}\right), \quad (3)$$

$$V_{C}(r) = \begin{cases} \frac{Z_{p}Z_{t}e^{2}}{2R_{C}}\left[3 - \left(\frac{r}{R_{C}}\right)^{2}\right], r < R_{C} \\ \frac{Z_{p}Z_{t}e^{2}}{r}, r \geq R_{C} \end{cases}, \quad (4)$$

$$R_{C} = r_{C}\left(A_{p}^{1/3} + A_{t}^{1/3}\right), \quad (5)$$

where $V_{C}(r)$ is the Coulomb potential, R_{C} is the Coulomb barrier radius with parameter r_{C}; Z_{p} and Z_{t} are the charges of the projectile and target, respectively; $V_{V,W}$ are the depths of the real and imaginary parts of the potential, respectively; $R_{V,W}$, $r_{V,W}$, and $a_{V,W}$ are their corresponding geometric parameters; A_{p} and A_{t} are the mass numbers of the projectile and target nuclei, respectively.

Table 1. Parameters of the optical potential (1) used in DWBA calculations for the specified entrance and exit channels [18]. See text for details.

Reaction Channel	V_{V} (MeV)	r_{V} (fm)	a_{V} (fm)	V_{W} (MeV)	r_{W} (fm)	a_{W} (fm)	r_{C} (fm)
^{3}He + ^{9}Be	103.9	0.7	0.777	23.81	0.854	0.817	0.767
α + ^{8}Be$_{gs}$	121.0	0.252	1.010	17.0 (14.9 [1])	1.38	0.34	0.724
α + ^{8}Be$_{3.03}$	121.0	0.252	1.010	17.0 (8.70 [1])	1.38	0.34	0.724

[1] The values obtained in this study.

As can be seen from Figure 2, curves DWBA-1 calculated using the entrance and exit channel potentials with the parameters from Ref. [18] differ just a little from the experimental data for the ^{9}Be(^{3}He, α)^{8}Be$_{gs}$ reaction channel but underestimate the data on the ^{9}Be(^{3}He, α)^{8}Be$_{3.03}$ reaction channel in the angular range of 30–90°. Such a discrepancy between the DWBA calculations and the experimental data can be eliminated either by varying the values of the spectroscopic amplitudes or by reducing the depth V_W of the imaginary part of the exit channel potential [41,42]. We chose the second option because the values of the spectroscopic amplitudes were obtained in Ref. [18] within the framework of the shell model calculations. Therefore, for a better description of the experimental data, we reduced the depth V_W of the imaginary part of the exit channel potential (curves DWBA-2), i.e., V_W was obtained by fitting to the neutron transfer data. For the core–core potential (^{3}He + ^{8}Be), we used the parameters of the entrance channel potential. The parameters of the optical potential (1) obtained for the entrance and exit channels are presented in Table 1.

The potential parameters for the exit channel α + ^{8}Be were obtained through a χ^2 minimization procedure based on the experimental data for the same reaction channel ^{3}He(^{9}Be, α)^{8}Be with fixed spectroscopic amplitudes and potential parameters for the entrance channel, i.e., the elastic scattering channel ^{3}He + ^{9}Be. It was found that the parameters of the fitted potential have unusually low values r_V = 0.252 fm and a_W = 0.34 fm; however, these values are close to those found for the α + ^{8}Be system in Ref. [43].

The discrepancy between the calculated differential cross-sections and the experimental data for the ^{9}Be(^{3}He, α)^{8}Be$_{gs}$ reaction channel around the scattering angle of 55° in Figure 2a may be attributed to the following factors:

(i) The ^{8}Be and ^{9}Be nuclei have a pronounced α-cluster structure, which can be incorporated into three-body wave functions for better description of the data [2–4].
(ii) Thanks to its α-cluster structure, the ^{9}Be nucleus has quite a deformation, while in this study, it was treated as spherical for simplicity [44].
(iii) It is possible that channel coupling effects are present, as observed in Refs. [17,45]. Indeed, the waves with different neutron transfer configurations, originating from multiple channels (e.g., from the ground state and the first excited state), may either cancel each other out or amplify one another; their interference can be taken into account.

Accounting for these factors may lead to an improved theoretical description of the experimental data, but goes beyond the scope of this paper.

To describe the dynamics of the ^{9}Be(^{3}He, α)^{8}Be$_{gs}$ reaction channel within the TDSE approach, we used the potential obtained for the ^{3}He + ^{9}Be entrance channel (Table 1) and the shell model potentials from the DWBA calculations, which yielded curves DWBA-2 in Figure 2.

4. Formalism of the TDSE Approach

The theoretical approach is based on the numerical solution of the time-dependent Schrödinger equation [28–31]:

$$i\hbar\frac{\partial}{\partial t}\Psi\left(\vec{r},t\right) = -\frac{\hbar^2}{2m}\Delta\Psi\left(\vec{r},t\right) + \\ +\left\{V_1\left(\left|\vec{r}-\vec{r}_1(t)\right|\right) + V_2\left(\left|\vec{r}-\vec{r}_2(t)\right|\right) + \hat{V}_{LS}^{(1)}\left(\vec{r}-\vec{r}_1(t)\right) + \hat{V}_{LS}^{(2)}\left(\vec{r}-\vec{r}_2(t)\right)\right\}\Psi\left(\vec{r},t\right), \quad (6)$$

where $\Psi\left(\vec{r},t\right)$ is the wave function of the neutron with mass m; $\vec{r}_1(t)$, $\vec{r}_2(t)$ are the centers of nuclei moving along classical trajectories; V_1, V_2 are the potentials of the interaction of the neutron with the projectile and target nuclei; $\hat{V}_{LS}^{(1)}$, $\hat{V}_{LS}^{(2)}$ are the potentials of the spin–orbit interaction of the neutron with the cores; $\hbar$ is the reduced Planck constant, t denotes the time.

As mentioned above, the neutron wave function at the initial moment of time was determined in the shell model with the parameters obtained in Section 3 and providing the energy of the single-particle level $1p_{3/2}$ equal to the experimental value of the neutron

separation energy (1.66 MeV) for the ^{9}Be nucleus [46]. The shape of the ^{9}Be nucleus was considered spherical [28–30] as soon as taking into account the deformation of ^{9}Be [47] requires more complex calculations, which will be the subject of a separate theoretical investigation in the future. In addition, it should be noted that taking into account the deformation of weakly bound nuclei in the calculations within the TDSE approach does not have a sensitive effect on the resulting probabilities and cross-sections of transfer reaction channels [28,29]. One of the reasons is that the wave functions calculated in the shell model for deformed and spherical nuclei have similar spatial extents due to the low binding energy of an outer neutron in such nuclei [48].

The wave function $\Psi\left(\vec{r},t\right)$ of the neutron with the projection j_z of the total momentum on z axis at the initial moment of time can be written as

$$\widetilde{\Psi}^{(0)}_{j_z}(\vec{r},t=0)=\begin{bmatrix}\widetilde{\psi}^{(0)}_{j_z}(\vec{r},t=0)\\ \widetilde{\varphi}^{(0)}_{j_z}(\vec{r},t=0)\end{bmatrix}=\begin{bmatrix}\psi^{(0)}_{j_z}\left\{\vec{r}-\vec{r}_2(t=0)\right\}\\ \varphi^{(0)}_{j_z}\left\{\vec{r}-\vec{r}_2(t=0)\right\}\end{bmatrix}\exp\left[i\hbar^{-1}m\vec{v}_2(t=0)\vec{r}\right], \tag{7}$$

where $\widetilde{\Psi}$ and $\widetilde{\varphi}$ are the components of the spinor wave function for the spin projections 1/2 and –1/2, respectively; $v_2(t)$ is the velocity of the target nucleus in the center of the mass system [28–30]. The evolution of the probability density $\rho(\vec{r},t)$ is calculated as

$$\rho(\vec{r},t)=\frac{1}{(2j+1)}\sum_{-j_z}^{j_z}\left|\psi_{j_z}(\vec{r},t)\right|^2+\left|\varphi_{j_z}(\vec{r},t)\right|^2. \tag{8}$$

For the neutron from the single-particle level $1p_{3/2}$ of the ^{9}Be nucleus, the values of j_z are –3/2, –1/2, 1/2, and 3/2.

The probability of the neutron transfer is determined as

$$P_{\mathrm{tr}}(t)=\sum_k|a_k(t)|^2, \tag{9}$$

$$a_k(t)=\int\left[\widetilde{\psi}^*_k(\vec{r},t)\psi(\vec{r},t)+\widetilde{\varphi}^*_k(\vec{r},t)\varphi(\vec{r},t)\right]dV, \tag{10}$$

where $a_k(t)$ are the amplitudes of the probabilities of populating the unoccupied single-particle neutron levels [30]. The final probability of the neutron transfer is determined at time t, when the nuclei are already far away from each other, in our calculations, at distances more than 30 fm:

$$\overline{P}_{\mathrm{tr}}=\lim_{t\to\infty}P_{\mathrm{tr}}(t). \tag{11}$$

The calculated probabilities $\overline{P}_{\mathrm{tr}}$ were approximated by the exponential function of the distance of the closest approach R_{min} [26]

$$\overline{P}_{\mathrm{tr}}(R_{\mathrm{min}})=\min\{\exp(A_0-B_0R_{\mathrm{min}}),1\} \tag{12}$$

with fitting parameters A_0 and B_0.

The probability of the removal of the neutron is determined as

$$P_{\mathrm{rem}}(t)=1-|c(t)|^2, \tag{13}$$

$$c(t)=\frac{1}{(2j+1)}\sum_{-j'_j}^{j'_z}\sum_{-j_z}^{j_z}\int\left[\widetilde{\psi}^{(0)*}_{j'_z}(\vec{r},t)\psi_{j_z}(\vec{r},t)+\widetilde{\varphi}^{(0)*}_{j'_z}(\vec{r},t)\varphi_{j_z}(\vec{r},t)\right]dV, \tag{14}$$

where $c(t)$ is the amplitude of the probability of conservation of the neutron in the initial state at time t [30]. Similar to the probability of the neutron transfer (11), the final probability

of the neutron removal is determined at time t, when the nuclei are already far away from each other:

$$\overline{P}_{\text{rem}} = \lim_{t\to\infty} P_{\text{rem}}(t). \quad (15)$$

The calculated probabilities $\overline{P}_{\text{rem}}$ were approximated by the sum of two exponential functions:

$$\overline{P}_{\text{rem}}(R_{\min}) = \min\{\exp(a_1 - b_1 R_{\min}) + \exp(a_2 - b_2 R_{\min}), 1\} \quad (16)$$

with fitting parameters A_1, B_1, A_2, B_2 [26].

The numerical solution of Equation (4) was performed on a spatial grid of dimensions (96 × 60 × 105) fm^3 ($x \times y \times z$) with the collision plane x0z and a grid step 0.3 fm [28–30]. We used the dimensionless time scale $\tau = t/t_0$, where $t_0 = mx_0^2/\hbar = 1.57 \times 10^{-23}$ s, $x_0 = 1$ fm. The dimensionless time step was $\Delta\tau = 0.1$. The calculations were carried out using the heterogeneous computing cluster HybriLIT [49] of the Laboratory of Information Technologies, Joint Institute for Nuclear Research.

5. Results and Discussion

The evolution of the probability density (6) in dimensionless time τ for the neutron from the single-particle level $1p_{3/2}$ of the ^{9}Be nucleus during the collision of ^{3}He + ^{9}Be at an energy E_{lab} = 30 MeV (the center-of-mass energy $E_{\text{c.m.}}$ = 22.5 MeV) with the impact parameter b = 6 fm ($R_{\min}$ = 6.12 fm) and b = 8 fm ($R_{\min}$ = 8.23 fm) is presented in Figures 3 and 4, respectively. The transition of the neutron probability density begins when the distance between the centers of the nuclei decreases to 9–10 fm (Figures 3a and 4a). As can be seen from Figures 3b and 4b, the relative velocity of the nuclei is high enough that the flux of the neutron probability density lags behind the motion of the two nuclei and is shifted relative to the imaginary line connecting their centers. A more intense rearrangement of the probability density occurs at quite small distances between the projectile and the target. As the distance between the nuclei increases, the neutron transfer is accompanied by the neutron transition to the continuum (Figures 3c and 4c) [34]. In Figures 3c and 4c, the neutron is emitted at a relatively large angle to the direction of motion of the projectile nucleus, which indicates the manifestation of the so-called *towing mode* at energies above 5 MeV/nucleon [34,50,51].

According to the shell model, the ^{3}He nucleus has only one single-particle level $1s_{1/2}$ that can be occupied by the neutron transferred from the single-particle level $1p_{3/2}$ of the ^{9}Be nucleus. The spherically symmetric shape of the part of the neutron probability density transferred to the ^{3}He projectile nucleus in Figures 3d and 4d indicates the population of the state $1s_{1/2}$ in ^{3}He, which is consistent with the shell model.

The obtained dependencies of the probability $\overline{P}_{\text{tr}}$ (11) and (12) on the distance $R_{\min}$ of the closest approach of the centers of the nuclei are shown in Figure 5a; the values of the fitting parameters are A_0 = 0.696 and B_0 = 0.515 fm^{-1}.

The obtained dependencies of the neutron removal probability $\overline{P}_{\text{rem}}$ (15) and (16) on the distance $R_{\min}$ of the closest approach of the centers of the nuclei are shown in Figure 5b; the values of the fitting parameters are A_1 = 1.178, B_1 = 0.362 fm^{-1}, A_2 = –2.08, B_2 = 0.011 fm^{-1}. The first exponential function describes a rapid decrease in the probability $\overline{P}_{\text{rem}}$ at the values of $R_{\min}$, not quite exceeding the Coulomb barrier radius; the second corresponds to a slow decrease at larger values and gives the main contribution at $R_{\min}$ more than 9 fm. The rapid decrease in the probability $\overline{P}_{\text{rem}}$ is due to a sharp decrease in the probability of the neutron transfer $\overline{P}_{\text{tr}}$ with the increasing impact parameter.

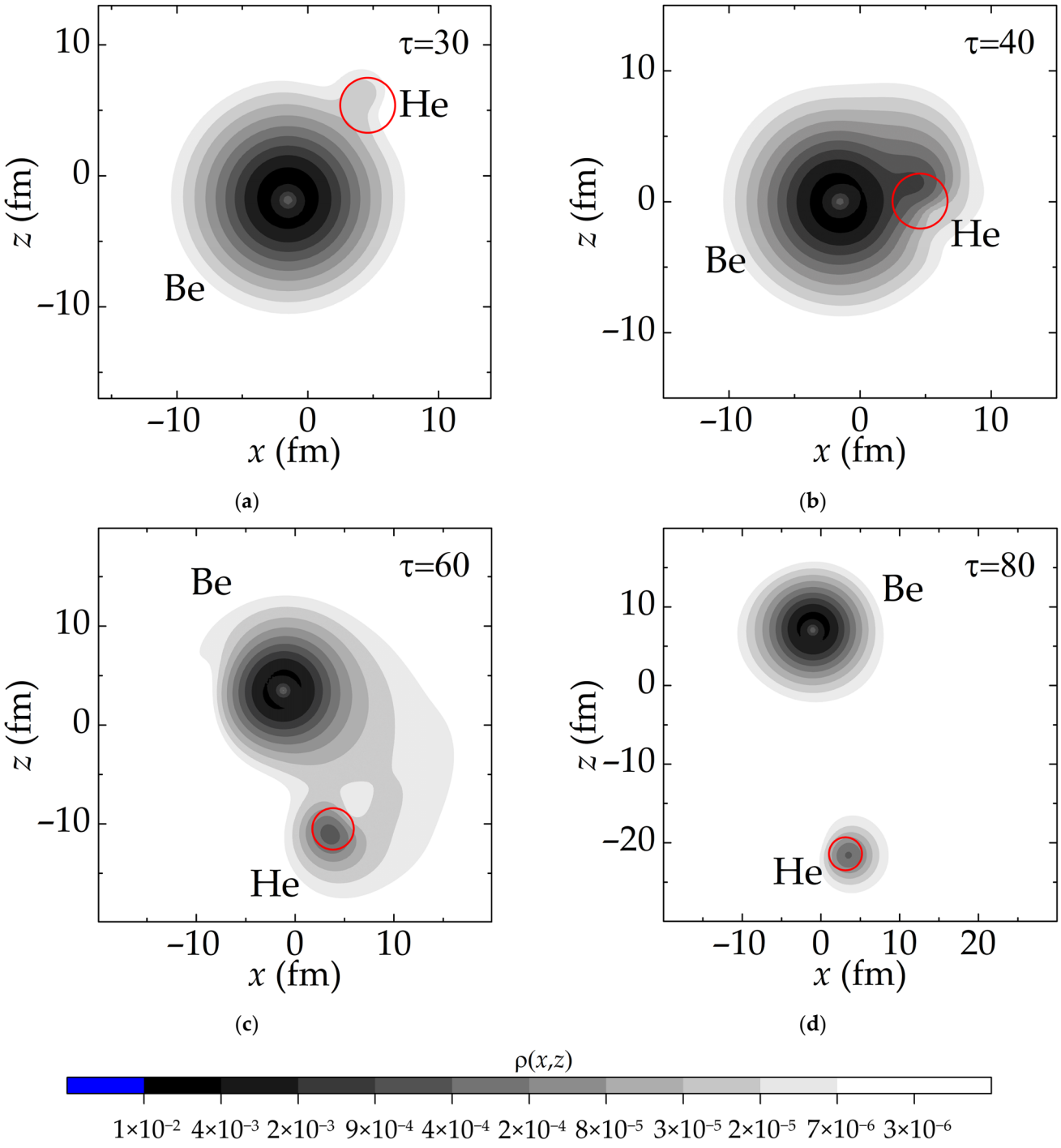

Figure 3. Evolution of the probability density $\rho(x,z)$ (in logarithmic scale; x and z are the coordinates in the collision plane) in dimensionless time τ = 30 (**a**), 40 (**b**), 60 (**c**), and 80 (**d**) for the neutron from the single-particle level $1p_{3/2}$ of the ^{9}Be nucleus during the collision of ^{3}He + ^{9}Be at an energy E_{lab} = 30 MeV (the center-of-mass energy $E_{\mathrm{c.m.}}$ = 22.5 MeV) with the impact parameter b = 6 fm (the distance of the closest approach R_{min} = 6.12 fm). The red circles indicate the imaginary boundary of the ^{4}He nucleus with a radius of 2 fm.

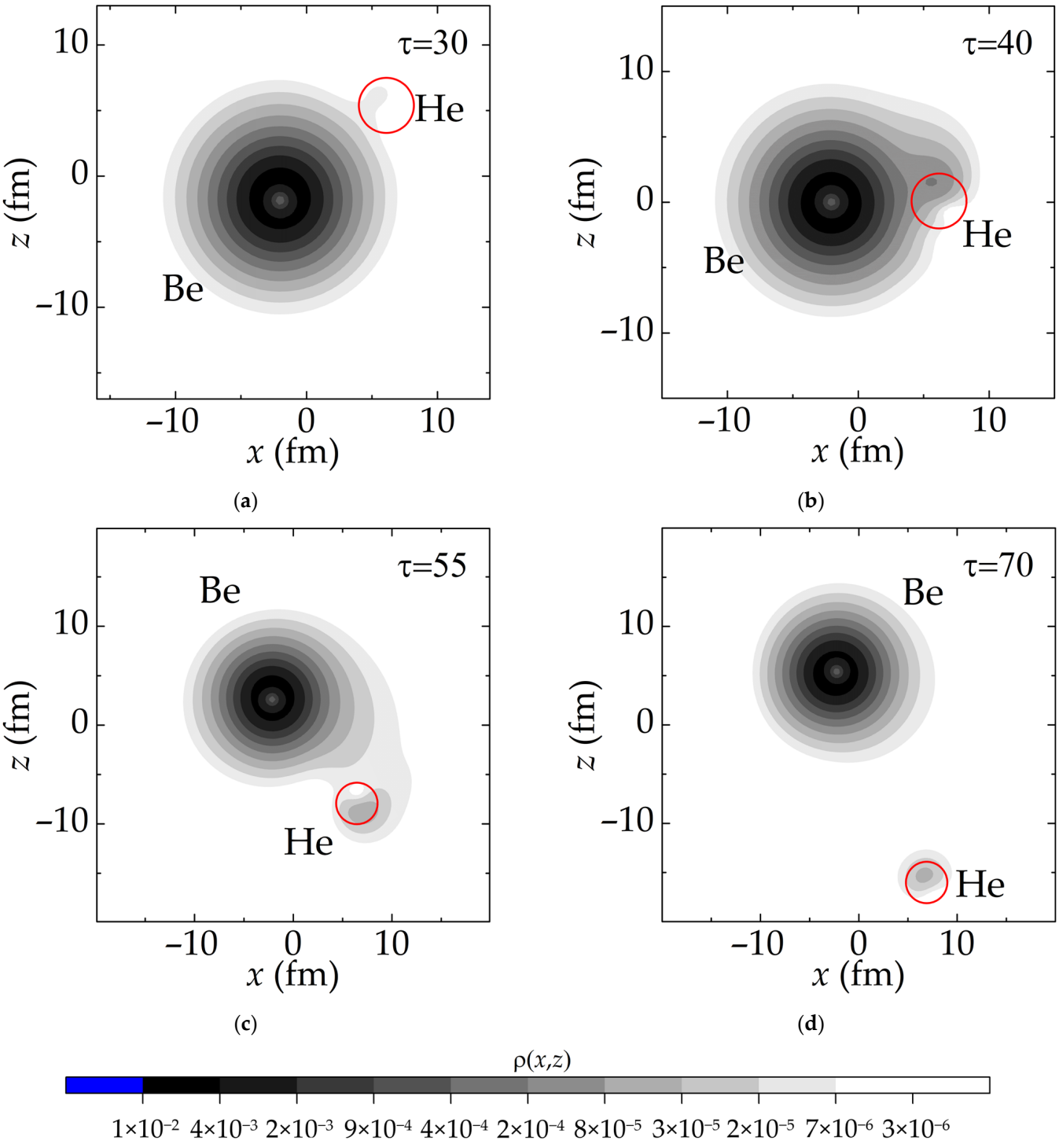

Figure 4. Same as Figure 3, but for b = 8 fm (R_{min} = 8.23 fm).

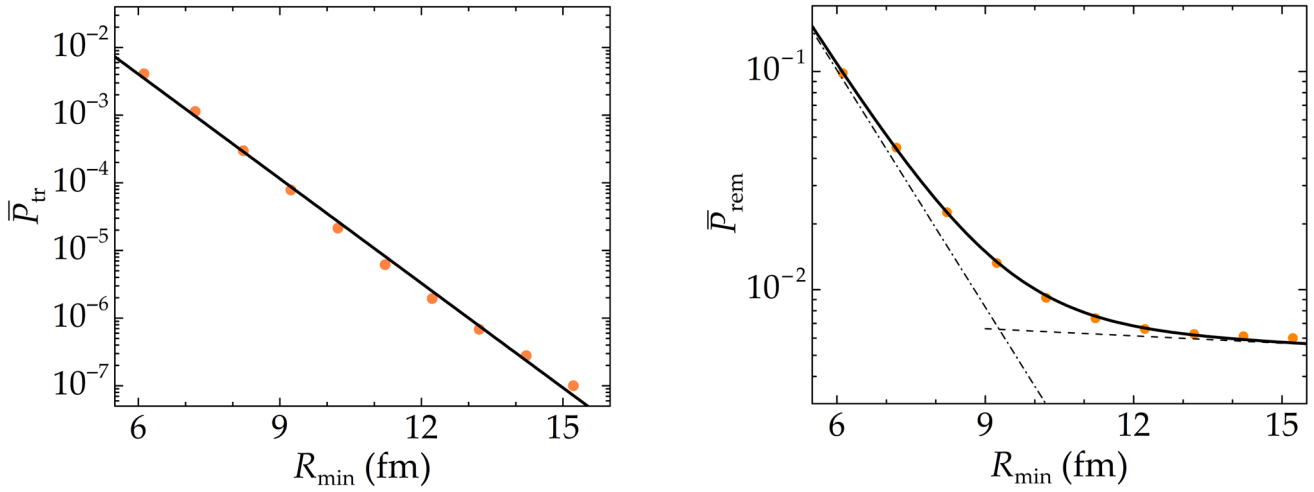

Figure 5. (**a**) The final neutron transfer probability $\overline{P}_{tr}$: circles are the result of calculations using Equation (11); line is the result of approximation (12). (**b**) The final neutron removal probability $\overline{P}_{rem}$: circles are the result of calculations using Equation (15); solid curve is the result of approximation (16); dashed and dash-dotted lines are the respective contributions of the exponential functions with a_1, b_1, and a_2, b_2 to approximation (16).

In the TDSE approach, the cross-sections for the transfer and removal of the weakly bound neutron of the ^{9}Be nucleus were calculated by integrating over the impact parameter b [29,31]

$$\sigma_{tr} = 2\pi \int_{b_{min}}^{\infty} \overline{P}_{tr}[R_{min}(b)]bdb, \quad (17)$$

$$\sigma_{rem} = 2\pi \int_{b_{min}}^{\infty} \overline{P}_{rem}[R_{min}(b)]bdb \quad (18)$$

where b_{min} is the impact parameter corresponding to the trajectory when the projectile is still captured by the target. In our calculations, we used b_{min} corresponding to $R_{min} = R_C + d$, where $R_C = 5.6$ fm and $d = 0.4$ fm is the diffuse region, and therefore $R_{min} = 6$ fm.

The comparison of the integrated cross-sections σ_{tr} for the reaction channel ^{9}Be(^{3}He, α)^{8}Be$_{gs}$ obtained within the DWBA (FRESCO code) and within the TDSE approach is presented in Table 2. One can see that the calculations in both models give close values. Taking into account that the differential cross-sections obtained within the DWBA are somewhat below the experimental points in the region of angles around 55°, one may conclude that the cross-sections (17) and (18) obtained within the TDSE approach are closer to the experimental data.

Table 2. Calculated cross-sections. See text for detais.

Reaction Channel	**^{9}Be(^{3}He, α)^{8}Be$_{gs}$**	**^{9}Be(^{3}He, α)^{8}Be$_{gs}$**	**^{9}Be(^{3}He, α)^{8}Be$_{3.03}$**	**^{9}Be + ^{3}He $\rightarrow$ ^{8}Be$_{gs}$**
Cross-section (mb)	σ_{tr} (gs, DWBA) 0.594	σ_{tr} (gs, TDSE) 0.740	σ_{tr} (3.03, DWBA) 1.375	σ_{rem} (TDSE) 315.690

The integrated cross-section σ_{tr} for the reaction channel ^{9}Be(^{3}He, α)^{8}Be$_{3.03}$ obtained within the DWBA is also presented in Table 2. The cross-section value for this reaction channel is approximately twice as high as that for ^{9}Be(^{3}He, α)^{8}Be$_{gs}$, which is consistent with the measured energy spectrum (Figure 1b), where the number of events for ^{8}Be$_{3.03}$ is approximately twice as high as that for ^{8}Be$_{gs}$.

Table 2 also includes the integrated cross-section σ_{rem} (18) obtained within the TDSE approach. According to Equation (13), σ_{rem} = 315.690 mb includes the neutron transfer cross-section σ_{tr} = 0.740 mb in the reaction channel ^{9}Be(^{3}He, α)^{8}Be$_{gs}$ and the cross-section for the transition of the neutron into the continuum. One can find that cross-section σ_{tr} contributes significantly to the cross-section σ_{rem}.

6. Conclusions

The angular distributions for the neutron transfer channels ^{9}Be(^{3}He, α)^{8}Be$_{gs,3.03}$ in the reaction of the ^{3}He (30 MeV) ions with the ^{9}Be target were measured. The experimental data were described by the DWBA using FRESCO code. The results of the theoretical description are found to be in agreement with the measurements. The parameters of the potentials for the ^{3}He + ^{9}Be entrance channel and for the shell model obtained from the DWBA calculations were successfully used in the description of dynamics of the reaction channel ^{9}Be(^{3}He, α)^{8}Be$_{gs}$ within the TDSE approach. It has been shown that the neutron transfer process begins when the nuclei approach each other at a distance of 9–10 fm between the centers of the nuclei, and the transfer process is accompanied by the transition of the neutron to the continuum. In addition, the neutron can be emitted at quite a large angle to the direction of motion of the projectile nucleus, which indicates the manifestation of the so-called *towing mode*.

The neutron transfer cross-section is found to not significantly contribute to the cross-section for the removal of the weakly bound neutron of the ^{9}Be nucleus. Calculations of the cross-section for the reaction channel ^{9}Be(^{3}He, α)^{8}Be$_{gs}$ in the TDSE approach and DWBA give close values.

Author Contributions: Conceptualization, A.K.A., E.K.A., M.A.N. and K.O.M.; methodology, T.G.I.; software, A.K.A. and E.K.A.; validation, A.K.A., S.M.L. and M.A.N.; formal analysis, M.A.N. and K.D.; investigation, A.K.A., T.G.I., B.A.U., K.D., A.M.K., S.M.L. and K.O.M.; resources, K.O.M. and T.K.Z.; data curation, T.G.I., K.O.M. and T.K.Z.; writing—original draft preparation, K.O.M.; writing—review and editing, K.O.M., A.K.A. and M.A.N.; visualization, E.K.A. and B.A.U.; supervision, A.K.A.; project administration, K.O.M.; funding acquisition, T.K.Z., K.D. and K.O.M. All authors have read and agreed to the published version of the manuscript.

Funding: This research was funded by the Science Committee of the Ministry of Science and Higher Education of the Republic of Kazakhstan, grant number AP14870958.

Data Availability Statement: All data obtained during the study are included in this paper. For any questions regarding the data in the paper, you can contact the corresponding authors.

Acknowledgments: We thank the team of the HybriLIT computing cluster (Laboratory of Information Technologies, Joint Institute for Nuclear Research, Dubna, Russia) for the opportunity to use its resources.

Conflicts of Interest: The authors declare no conflicts of interest.

References

1. Villanueva, G.; Moro, A.M.; Casal, J.; Lei, J. Neutron-transfer induced breakup of the Borromean nucleus ^{9}Be. *Phys. Lett. B* **2024**, *855*, 138766. [CrossRef]
2. Fulton, B.R.; Cowin, R.L.; Woolliscroft, R.J.; Clarke, N.M.; Donadille, L.; Freer, M.; Leask, P.J.; Singer, S.M.; Nicoli, M.P.; Benoit, B.; et al. Exclusive breakup measurements for ^{9}Be. *Phys. Rev. C* **2004**, *70*, 047602. [CrossRef]
3. Prezado, Y.; Borge, M.J.G.; Diget, C.A.; Fraile, L.M.; Fulton, B.R.; Fynbo, H.O.U.; Jeppesen, H.B.; Jonson, B.; Meister, M.; Nilsson, T.; et al. Low-lying resonance states in the ^{9}Be continuum. *Phys. Lett. B* **2005**, *618*, 43–50. [CrossRef]
4. Álvarez-Rodríguez, R.; Jensen, A.S.; Garrido, E.; Fedorov, D.V. Structure and three-body decay of ^{9}Be resonances. *Phys. Rev. C* **2010**, *82*, 034001. [CrossRef]
5. Soukeras, V.; Sgouros, O.; Pakou, A.; Cappuzzello, F.; Casal, J.; Agodi, C.; Brischetto, G.A.; Calabrese, S.; Carbone, D.; Cavallaro, M.; et al. Global study of ^{9}Be + p at 2.72A MeV. *Phys. Rev. C* **2020**, *102*, 064622. [CrossRef]
6. von Oertzen, W.; Freer, M.; Kanada-En'yo, Y. Nuclear clusters and nuclear molecules. *Phys. Rep.* **2006**, *432*, 43–113. [CrossRef]
7. Freer, M. The clustered nucleus—Cluster structures in stable and unstable nuclei. *Rep. Prog. Phys.* **2007**, *70*, 2149–2210. [CrossRef]
8. Samarin, V.V. Study of spatial structures in α-cluster nuclei. *Eur. Phys. J. A* **2022**, *58*, 117. [CrossRef]

9. Bazhin, A.S.; Samarin, V.V. Study of the structure of the ^{9}Be nucleus in the alpha-cluster model by the method of hyperspherical functions. *Bull. Russ. Acad. Sci. Phys.* **2024**, *88*, 1177–1184. [CrossRef]
10. Rakityansky, S.A. Wave function of ^{9}Be in the three-body ($\alpha\alpha$n) model. *Phys. Rev. C* **2024**, *110*, 024001. [CrossRef]
11. Tilley, D.R.; Kelley, J.H.; Godwin, J.L.; Millener, D.J.; Purcell, J.E.; Sheu, C.G.; Weller, H.R. Energy levels of light nuclei A = 8,9,10. *Nucl. Phys. A* **2004**, *745*, 155–362. [CrossRef]
12. Nyman, G.; Azuma, R.E.; Hansen, P.G.; Jonson, B.; Larsson, P.O.; Mattsson, S.; Richter, A.; Riisager, K.; Tengblad, O.; Wilhelmsen, K.; et al. The beta decay of ^{9}Li to levels in ^{9}Be: A new look. *Nucl. Phys. A* **1990**, *510*, 189–208. [CrossRef]
13. Keeley, N.; Alamanos, N.; Rusek, K.; Kemper, K.W. Generation of a repulsive dynamic polarization potential by transfer couplings. *Phys. Rev. C* **2005**, *71*, 014611. [CrossRef]
14. Pandit, S.K.; Jha, V.; Mahata, K.; Santra, S.; Palshetkar, C.S.; Ramachandran, K.; Parkar, V.V.; Shrivastava, A.; Kumawat, H.; Roy, B.J.; et al. Investigation of cluster structure of ^{9}Be from high precision elastic scattering data. *Phys. Rev. C* **2011**, *84*, 031601. [CrossRef]
15. Saduyev, N.; Nassurlla, M.; Burtebayev, N.; Sakuta, S.; Nassurlla, M.; Kalikulov, O.; Khojayev, R.; Sabidolda, A.; Issayev, D. Scattering and one neutron pick-up reaction on a ^{10}B target with deuterons at an energy of 14.5 MeV. *Physics* **2024**, *6*, 1098–1110. [CrossRef]
16. Lukyanov, S.M.; Harakeh, M.N.; Naumenko, M.A.; Xu, Y.; Trzaska, W.H.; Burjan, V.; Kroha, V.; Mrazek, J.; Glagolev, V.; Piskoř, Š.; et al. Cluster structure of ^{9}Be from ^{3}He + ^{9}Be reaction. *J. Phys. Conf. Ser.* **2016**, *724*, 012031. [CrossRef]
17. Urazbekov, B.A.; Denikin, A.S.; Lukyanov, S.M.; Itaco, N.; Janseitov, D.M.; Mendibayev, K.; Burjan, V.; Kroha, V.; Mrazek, J.; Trzaska, W.H.; et al. Clusterization and strong coupled-channels effects in deuteron interaction with ^{9}Be nuclei. *J. Phys. G* **2019**, *46*, 105110. [CrossRef]
18. Urazbekov, B.; Issatayev, T.; Lukyanov, S.; Azhibekov, A.; Denikin, A.; Mendibayev, K.; Janseitov, D.; Penionzhkevich, Y.; Kuterbekov, K.; Zholdybayev, T. Reactions induced by 30 MeV ^{3}He beam on ^{9}Be: Cluster transfer reactions. *Chin. Phys. C* **2023**, *48*, 014001. [CrossRef]
19. Azhibekov, A.K.; Lukyanov, S.M.; Penionzhkevich, Y.E.; Urazbekov, B.A.; Naumenko, M.A.; Samarin, V.V.; Issatayev, T.; Maslov, V.A.; Mendibayev, K.; Aznabayev, D.; et al. Study of one-step and two-step neutron transfer in the reaction ^{6}Li + ^{9}Be. *Chin. Phys. C* **2024**, *48*, 114101. [CrossRef]
20. Urazbekov, B.A.; Denikin, A.S.; Sakhiev, S.K.; Burtebaev, N.T. Manifestation of the cluster structure of the ^{9}Be nucleus in direct nuclear reactions. *Bull. Russ. Acad. Sci. Phys.* **2016**, *80*, 247–251. [CrossRef]
21. Urazbekov, B.A.; Denikin, A.S.; Sakhiev, S.K.; Lukyanov, S.M. Studying the reactions of deuteron interaction with ^{9}Be nuclei at low energies. *Bull. Russ. Acad. Sci. Phys.* **2017**, *81*, 690–694. [CrossRef]
22. Bilwes, B.; Bilwes, R.; Ferrero, J.L.; Garcia, A. Mécanisme de la réaction ^{9}Be(^{3}He, α)^{8}Be(o) et résonances géantes isoscalaires du ^{12}C. *J. Phys. Fr.* **1978**, *39*, 805–814. [CrossRef]
23. Karban, O.; Basak, A.K.; England, J.B.A.; Morrison, G.C.; Nelson, J.M.; Roman, S.; Shute, G.G. The j-dependence of (^{3}He, d) and (^{3}He, α) reaction analysing powers in the 1p shell. *Nucl. Phys. A* **1976**, *269*, 312–326. [CrossRef]
24. Moazed, C.; Holmgren, H.D. Angular Correlations for the Reaction ^{9}Be(^{3}He, α)^{8}Be (16.92) $\rightarrow$ α + α. *Phys. Rev. B* **1968**, *166*, 977–987. [CrossRef]
25. Satchler, G.R. *Direct Nuclear Reactions*; Oxford University Press: New York, NY, USA, 1983.
26. Taylor, J.R. *Scattering Theory: The Quantum Theory of Nonrelativistic Collisions*; Dover Publications, Inc.: Mineola, NY, USA, 2006.
27. Thompson, I.J. Coupled reaction channels calculations in nuclear physics. *Comput. Phys. Rep.* **1988**, *7*, 167–212. [CrossRef]
28. Azhibekov, A.K.; Samarin, V.V.; Kuterbekov, K.A. Time-dependent calculations for neutron transfer and nuclear breakup processes in ^{11}Li + ^{9}Be and ^{11}Li + ^{12}C reactions at low energy. *Chin. J. Phys.* **2020**, *65*, 292–299. [CrossRef]
29. Azhibekov, A.K.; Samarin, V.V. Time-dependent description of reactions with weakly bound ^{11}Li and ^{11}Be nuclei. *Bull. Russ. Acad. Sci. Phys.* **2022**, *86*, 1092–1098. [CrossRef]
30. Azhibekov, A.K.; Lukyanov, S.M.; Shakhov, A.V.; Penionzhkevich, Y.E.; Naumenko, M.A.; Devaraja, H.M.; Almanbetova, E.K.; Urazbekov, B.A.; Bodrov, A.Y.; Mardyban, E.V.; et al. Neutron transfer in the ^{48}Ca + ^{197}Au reaction. *Eur. Phys. J. A* **2023**, *59*, 278. [CrossRef]
31. Samarin, V.V. Time-dependent description of incomplete fusion of nuclei and cluster and nucleon-transfer reactions. *Phys. At. Nucl.* **2018**, *81*, 486–496. [CrossRef]
32. Valiolda, D.; Janseitov, D.; Melezhik, V. Investigation of low-lying resonances in breakup of halo nuclei within the time-dependent approach. *Eur. Phys. J. A* **2022**, *58*, 34. [CrossRef]
33. Samarin, V.V.; Naumenko, M.A. Study of nucleon-transfer processes in low-energy reactions of helium isotopes with ^{197}Au nuclei. *Phys. At. Nucl.* **2022**, *85*, 880–889. [CrossRef]
34. Lima, V.; Scarpaci, J.; Lacroix, D.; Blumenfeld, Y.; Bourgeois, C.; Chabot, M.; Chomaz, P.; Désesquelles, P.; Duflot, V.; Duprat, J.; et al. Nuclear break-up of ^{11}Be. *Nucl. Phys. A* **2007**, *795*, 1–18. [CrossRef]
35. Kukulin, V.I.; Voronchev, V.T. Pinch-based thermonuclear D^{3}He fusion driven by a femtosecond laser. *Phys. At. Nucl.* **2010**, *73*, 1376–1383. [CrossRef]
36. Seksembayev, Z.; Kukulin, V.; Sakhiyev, S. Study of a dense hot plasma's burning in Z-pinch devices with inertial-magnetic confinement. *Phys. Scr.* **2018**, *93*, 085602. [CrossRef]

37. Sgouros, O.; Soukeras, V.; Pakou, A. Low energy proton induced reactions with weakly bound nuclei for application purposes. *Eur. Phys. J. A* **2021**, *57*, 125. [CrossRef]
38. Tun, Z.; Yamani, Z.; Huang, X.; Li, G.; Hartling, K.; Horn, D. Liquid-lithium-cooled beryllium target as the p-to-n converter. *Nucl. Instrum. Methods Phys. Res. A Accel. Spectrom. Detect. Assoc. Equip.* **2024**, *1064*, 169459. [CrossRef]
39. The Main Upgrades of the Cyclotron U-120M. Physics Institute CAS: Řež, Czech Republic. 2023. Available online: https://www.ujf.cas.cz/en/departments/department-of-accelerators/cyclotron/ (accessed on 30 October 2024).
40. Janseitov, D.M.; Lukyanov, S.M.; Mendibayev, K.; Penionzhkevich, Y.E.; Skobelev, N.K.; Sobolev, Y.G.; Kuterbekov, K.A.; Valiolda, D.S.; Zholdybayev, T.K.; Trzaska, W.H.; et al. Investigation of the elastic and inelastic scattering of ^{3}He from ^{9}Be in the energy range 30–60 MeV. *Int. J. Mod. Phys. E* **2018**, *27*, 1850089. [CrossRef]
41. Micek, S.; Rebel, H.; Gils, H.J.; Klewe-Nebenius, H.; Zagromski, S.; Srivastava, D.K. Single nucleon transfer reactions in ^{6}Li + ^{6}Li collisions at 156 MeV. *Z. Phys. A* **1987**, *328*, 467–473. [CrossRef]
42. Ruby, L.; Pyle, R.V.; Wong, Y.-C. Cross sections for ^{6}Li(^{6}Li,^{5}He)^{7}Be, ^{6}Li(d, n)^{7}Be, and ^{19}F(^{6}Li, p)^{24}Na. *Nucl. Sci. Engin.* **1979**, *71*, 280–286. [CrossRef]
43. Cuong, D.C.; Descouvemont, P.; Khoa, D.T.; Phuc, N.H. Coupled-reaction-channel study of the ^{12}C(α, ^{8}Be) reaction and the ^{8}Be + ^{8}Be optical potential. *Phys. Rev. C* **2020**, *102*, 024622. [CrossRef]
44. Sundholm, D.; Olsen, J. Large MCHF calculations on the hyperfine structure of Be(^{3}P^{O}): The nuclear quadrupole moment of ^{9}Be. *Chem. Phys. Lett.* **1991**, *177*, 91–97. [CrossRef]
45. Harakeh, M.N.; Van Popta, J.; Saha, A.; Siemssen, R.H. Strong coupled-channels effects in the ^{9}Be(α, t)10B reaction. *Nucl. Phys. A* **1980**, *344*, 15–40. [CrossRef]
46. Wang, M.; Audi, G.; Wapstra, A.H.; Kondev, F.; MacCormick, M.; Xu, X.; Pfeiffer, B. The AME 2012 atomic mass evaluation. *Chin. Phys. C* **2012**, *36*, 1603–2014. [CrossRef]
47. Chart of Nucleus Shape and Size Parameters. Centre for Photonuclear Experiments Data (CDFE), Skobeltsyn Institute of Nuclear Physics, Lomonosov Moscow State University (SINP MSU): Moscow, Russia. 2023. Available online: http://cdfe.sinp.msu.ru/services/radchart/radmain.html (accessed on 30 October 2024).
48. Azhibekov, A.K.; Samarin, V.V.; Kuterbekov, K.A.; Naumenko, M.A. Shell model calculations for deformed Li isotopes. *Euras. J. Phys. Funct. Mater.* **2019**, *3*, 307–318. [CrossRef]
49. Heterogeneous Platform "HybriLIT". Laboratory of Information Technologies, Joint Institute for Nuclear Research (LIT, JINR): Dubna, Russia. 2023. Available online: http://hlit.jinr.ru/ (accessed on 30 October 2024).
50. Scarpaci, J.; Beaumel, D.; Blumenfeld, Y.; Chomaz, P.; Frascaria, N.; Jongman, J.; Lacroix, D.; Laurent, H.; Lhenry, I.; Maréchal, F.; et al. A new phenomenon in heavy ion inelastic scattering: The towing mode. *Phys. Lett. B* **1998**, *428*, 241–247. [CrossRef]
51. Lacroix, D.; Scarpaci, J.A.; Chomaz, P. Theoretical description of the towing mode through a time-dependent quantum calculation. *Nucl. Phys. A* **1999**, *658*, 273–281. [CrossRef]